



Contents lists available at ScienceDirect

Bioorganic & Medicinal Chemistry

journal homepage: www.elsevier.com/locate/bmc

Design, biological evaluation and 3D QSAR studies of novel dioxin-containing triaryl pyrazoline derivatives as potential B-Raf inhibitors

Yu-Shun Yang^{a,b,†}, Bing Yang^{b,†}, Yan Zou^{a,b}, Guigen Li^{b,*}, Hai-Liang Zhu^{a,*}

^a State Key Laboratory of Pharmaceutical Biotechnology, Nanjing University, Nanjing 210023, China

^b Institute of Chemistry and BioMedical Sciences, School of Chemistry and Chemical Engineering, Nanjing University, Nanjing 210023, China

ARTICLE INFO

Article history:

Received 17 April 2016

Revised 10 May 2016

Accepted 11 May 2016

Available online xxxx

Keywords:

Break limit

Triaryl pyrazoline

Dioxin

Antitumor activity

B-Raf

Selective

3D QSAR

ABSTRACT

A series of novel dioxin-containing triaryl pyrazoline derivatives **C1–C20** have been synthesized. Their B-Raf inhibitory and anti-proliferation activities were evaluated. Compound **C6** displayed the most potent biological activity against B-Raf^{V600E} and WM266.4 human melanoma cell line with corresponding IC₅₀ value of 0.04 μM and GI₅₀ value of 0.87 μM, being comparable with the positive controls and more potent than our previous best compounds. Moreover, **C6** was selective for B-Raf^{V600E} from B-Raf^{WT}, C-Raf and EGFR and low toxic. The docking simulation suggested the potent bioactivity might be caused by breaking the limit of previous binding pattern. A new 3D QSAR model was built with the activity data and binding conformations to conduct visualized SAR discussion as well as to introduce new directions. Stretching the backbone to outer space or totally reversing the backbone are both potential orientations for future researches.

© 2016 Elsevier Ltd. All rights reserved.

1. Introduction

Thousands of times researchers claimed breakthroughs on treating cancer, yet cancer continues to play the role of health risker all over the world, ranked second in causing mortality.¹ Still, people are looking forward to novel anticancer agents and therapeutic methods although huge progress in medicine has been made.

As an important pathway for cell proliferation and survival,² Ras-Raf-MEK-ERK serine threonine kinase cascade, also called ERK/MAP kinase pathway or ‘classical’ MAPK pathway, has been reported to be hyper-activated in up to 30% of human cancers.^{3–6} Especially, activating mutations in Raf have been observed most, 50–70% of cell lines and tumors in melanoma, then 40–70% in thyroid cancer, 50–70% in ovarian cancer.^{7–9} Researchers regard B-Raf as a most important isoform of Raf kinases because approximately 90% of its activating mutations in cancers are valine for glutamic acid substitution (V600E, formally defined as V599E),^{7,10,11} which can cause a 500-fold increase in the basal rate of MEK phosphorylation over wild-type B-Raf^{WT} and consequently result in stimulating tumor growth and vascular endothelial growth factor

secretion.^{13,14} Therefore B-Raf has been considered as a hotspot in designing anticancer agents.^{15–17}

Now Vemurafenib is the top B-Raf inhibitor with FDA approval, but attempts in seeking alternative backbones to break the fixed structural limitation never stop.¹⁸ Previous reporters picked out triarylimidazole derivative SB-590885 as a potent B-Raf inhibitor.¹⁹ There exists a key interaction between heterocyclic rings (both imidazole and pyridine) of SB-590885 and PHE583 of B-Raf.¹⁹ To avoid the 7-azaindole moiety of Vemurafenib and eliminate the corresponding side effect, dihydropyrazole derivatives have been screened and convinced to be potent and selective inhibitors of B-Raf^{V600E}.^{20,21}

In our previous studies, a certain pattern of 1,3,5-triaryl-pyrazoline derivatives as B-Raf inhibitor has been screened out.^{22,23} Although the top compound was quite close to the positive control, the refined substitutes on 1, 3, 5 positions inferred the worry that this pattern might be reaching its own limitation. Meanwhile, we cannot ignore the dioxin moiety because it was the best choice on 1-position (ring C) of pyrazoline. Fortunately, in this pattern 3-position (ring A) and 1-position (ring C) were nearly in one plane while 5-position (ring B) had an angle with this plane. Meanwhile, a parallel report suggested the possibility of defaulting carbonyl.²⁴ Thus, here we do the challenging work to interchange ring A and ring C to break the limitation of former backbone, hoping to approach an appreciating situation.

* Corresponding authors. Tel./fax: +86 25 89682572.

E-mail addresses: guigenli@nju.edu.cn (G. Li), zhuhl@nju.edu.cn (H.-L. Zhu).

† Both authors contributed equally to the work.

2. Results and discussion

2.1. Chemistry

3-(2,3-Dihydrobenzo[*b*][1,4]dioxin-6-yl)-5-aryl-1-phenyl-4,5-dihydro-1*H*-pyrazole derivatives **C1–C20** were synthesized and screened for their antitumor activity. All of them were synthesized for the first time except **C1** whose synthesis was reported by Jonaitis group and Dauksas group respectively in 1960s.^{25,26} Their bioactivities were tested for the first time. The general synthesis method and the structures of compounds **C1–C20** were organized in Scheme 1. They were all prepared in two steps. Firstly, different substituted benzaldehydes on treatment with 1-(2,3-dihydrobenzo[*b*][1,4]dioxin-6-yl)ethan-1-one in presence of 50% NaOH were stirred at room temperature till reactions completed, yielding different analogues of chalcones (**B**). Secondly, phenylhydrazine was added to participate the cyclization of the obtained powder, leading to the corresponding target compounds **C1–C20** 3-(2,3-dihydrobenzo[*b*][1,4]dioxin-6-yl)-5-aryl-1-phenyl-4,5-dihydro-1*H*-pyrazoles. Subsequent purification with recrystallisation was conducted and the refined compounds were finally obtained. All of the synthetic compounds gave satisfactory analytical and spectroscopic data, which were in full accordance with their depicted structures.

2.2. Biological activity

All the synthesized compounds **C1–C20** were evaluated for their anti-proliferation effect and B-Raf^{V600E} inhibitory activity with a general method. The results were expressed as concentrations of IC₅₀ (the half maximal inhibitory concentration of B-Raf^{V600E} mediated MEK phosphorylation) and GI₅₀ (the half maximal inhibitory concentration of WM266.4 human melanoma cell line²⁷ growth), presented in Table 1. To make comparison with previous researches, we chose the same cell line WM266.4 and took two previous best compounds **COA** (named **C14** in previous work)²³ and **COB** (named **C6** in previous work)²⁴ into the same evaluation (both their test results and literature values). As shown in Table 1, a majority of the compounds still kept potent B-Raf^{V600E} inhibitory activity. It seemed that interchange ring A and ring C was an available and rational method.

The linear regression between the GI₅₀ values of these compounds shared a similar tendency with their relevant IC₅₀ values (*R* square = 0.879, a normal level) indicated the correlation between the anti-proliferative effect and the B-Raf inhibitory activity.

The most potent compound **C6** displayed comparable activity (IC₅₀ = 0.04 μM; GI₅₀ = 0.87 μM) with the positive controls Vemurafenib (IC₅₀ = 0.03 μM; GI₅₀ = 0.21 μM) and Erlotinib (IC₅₀ = 0.06 μM; GI₅₀ = 8.14 μM). The B-Raf inhibitory activity of **C6** seemed slightly better than the previous best compounds **COA** (IC₅₀ = 0.11 μM in test; IC₅₀ = 0.11 μM in literature) and **COB** (IC₅₀ = 0.14 μM in test; IC₅₀ = 0.15 μM in literature). An explanation for being less potent than **COA** on anti-proliferation might be the influence of log*P* and PSA (polar surface area) by defaulting carbonyl. The ADMET properties of **C1–C20** were shown in Figure 1, in which the properties of **C6** was not top class but good enough. Introducing appropriate pharmacokinetics groups could cover this disadvantage.

After molecular overlap (Fig. 2) and bioassay results being examined, preliminary SAR studies were provided to discuss how structure variation might affect anticancer activity. Firstly, we fixed R group with substituted phenyl but temporarily skipped benzyloxyphenyl group for the tortuosity of steric backbone. A single substitute on *meta*-position showed better effect than on *para*-position (**C7** > **C11**; **C5** > **C12**, here '>' means 'better than'); whereas

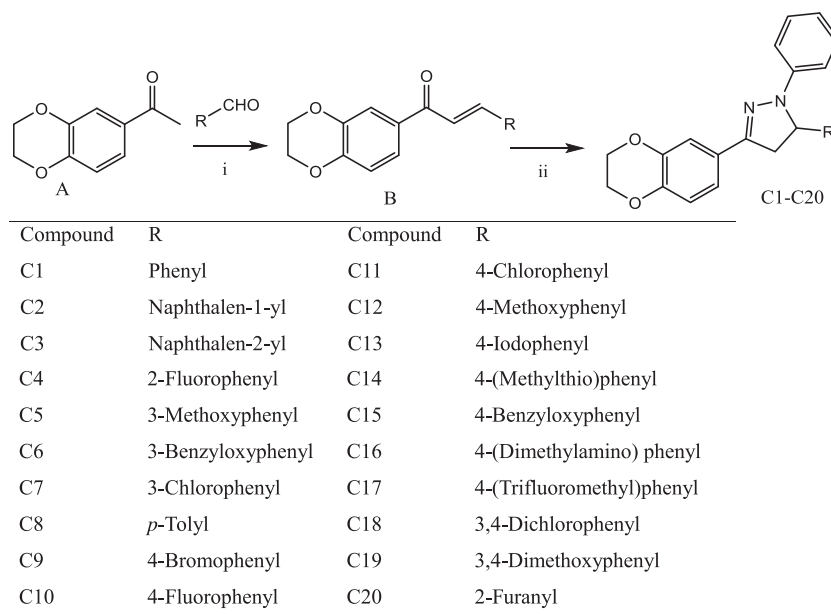
a same substitute on *para*-position seemed more potent than on *ortho*-position (**C10** > **C4**). As for *meta*-position, a slight tendency was –Cl > –OMe, indicating that an electron-withdrawing group might be better choice here. The corresponding compounds were **C7** (IC₅₀ = 0.15 μM) > **C5** (IC₅₀ = 0.21 μM). As for *para*-position, the inferred order was –N(Me)₂ > –Me > –Br > –I > –F > –SMe > –H > –Cl > –CF₃ > –OMe, indicating that a steric suitable substitute with slighter electronic influence should be recommended in future designing. The corresponding compounds were **C16** (IC₅₀ = 0.07 μM) > **C8** (IC₅₀ = 0.61 μM) > **C9** (IC₅₀ = 0.86 μM) > **C13** (IC₅₀ = 1.14 μM) > **C10** (IC₅₀ = 3.88 μM) > **C14** (IC₅₀ = 4.27 μM) > **C1** (IC₅₀ = 8.05 μM) > **C11** (IC₅₀ = 10.7 μM) > **C17** (IC₅₀ = 36.3 μM) > **C12** (IC₅₀ = 118 μM). 4-Dimethylamino showed an accidentally potency might because it was more like *meta*-substitutes. Meanwhile, as for multi substitutes, if they were on both *para*- and *meta*-positions, the effect was between a single *meta*-one and a single *para*-one. The corresponding compounds with –Cl and –OMe were **C7** (IC₅₀ = 0.15 μM) > **C18** (IC₅₀ = 0.27 μM) > **C11** (IC₅₀ = 10.7 μM) and **C5** (IC₅₀ = 0.21 μM) > **C19** (IC₅₀ = 0.54 μM) > **C12** (IC₅₀ = 118 μM), respectively. Secondly, naphthalene was not a fine group and Naphthalen-2-yl group showed better effect than Naphthalen-1-yl group as **C3** (IC₅₀ = 6.85 μM) > **C2** (IC₅₀ > 300 μM). This result agreed with the order of single substitutes (*meta*- > *para*- > *ortho*-). Thirdly, a heterocyclic ring (here it was furan) also seemed worse than benzene ring with the corresponding result **C1** (IC₅₀ = 8.05 μM) > **C20** (IC₅₀ = 83.6 μM). Finally, as for benzyloxyphenyl group, both 3-OBn and 4-OBn affected the backbone. However, 3-OBn only stretched the backbone while 4-OBn made the backbone reversed. Despite this difference and the slightly inferior ADMET properties (log*P* = 6.408, PSA = 41.666), both 3-OBn and 4-OBn showed accidentally admirable activity with the corresponding results **C6** (IC₅₀ = 0.04 μM) and **C15** (IC₅₀ = 0.11 μM) respectively. That meant the challenging design might break the limit on at least two orientations which could be interesting in future study. The data were visualized as maps and a more brief SAR analysis was displayed in the 3D QSAR part below.

To evaluate the selectivity of this series, the kinase inhibitory activities against B-Raf^{WT} (wild type B-Raf), C-Raf (also called Raf1), EGFR and the anti-proliferation effect against MCF-7 human breast cancer cell line of representative compounds (**C6**, **C16**, **C15**, **C7**, **C5** and **C18**) were tested. The results were provided in Table 2. For the most potent **C6**, the IC₅₀ value against B-Raf^{V600E} was 0.04 μM while that against B-Raf^{WT} was 1.06 μM. This result suggested that **C6** was relatively selective between B-Raf^{V600E} and B-Raf^{WT}. This scale of selectivity might be further considered in therapeutic method but was acceptable with appropriate dosage. From C-Raf or EGFR, all representative compounds indicated obvious selectivity for B-Raf^{V600E}. The anti-proliferation against MCF-7 in which V600E mutant merely happened also convinced the selectivity of representative compounds. The moderate anti-proliferation effect against MCF-7 might be from the moderate inhibitory activities against B-Raf^{WT} and C-Raf.

The cytotoxic activity of the compounds were evaluated on a mouse embryonic fibroblast cell line (NIH-3T3) using the MTT assay. The results were summarized in Table 2. It could be concluded that the selected compounds with potent inhibitory activity and high selectivity were low toxic.

2.3. Molecular docking

To visualize the possible binding model of interactions between a protein (enzyme) and small molecules (ligands) were the molecular docking techniques used.²⁸ Molecular modelling in this study was conducted by using CDocker protocol in Discovery Studio 3.5 (Discovery Studio 3.5, Accelrys, Inc. San Diego, CA). All twenty



Scheme 1. General synthesis of compounds (**C1–C20**). Reagents and conditions: (i) EtOH, 50% NaOH, TLC; (ii) EtOH, phenylhydrazine, reflux, overnight.

Table 1
B-Raf^{V600E} inhibitory activity and anti-proliferation activity of the synthesized compounds (**C1–C20**) as well as previous compounds **C0A** and **C0B**

Compounds	IC ₅₀ (μM) B-Raf ^{V600E}	GI ₅₀ (μM) WM266.4	Compounds	IC ₅₀ (μM) B-Raf ^{V600E}	GI ₅₀ (μM) WM266.4
C1	8.05 ± 0.73	22.4 ± 1.88	C11	10.7 ± 1.01	38.6 ± 3.42
C2	>300	>100	C12	118 ± 9.85	>100
C3	6.85 ± 0.57	13.9 ± 1.16	C13	1.14 ± 0.10	3.47 ± 0.29
C4	5.17 ± 0.49	9.12 ± 0.83	C14	4.27 ± 0.41	6.87 ± 0.64
C5	0.21 ± 0.02	1.81 ± 0.15	C15	0.11 ± 0.01	1.13 ± 0.11
C6	0.04 ± 0.003	0.87 ± 0.07	C16	0.07 ± 0.005	0.97 ± 0.08
C7	0.15 ± 0.01	1.75 ± 0.16	C17	36.3 ± 3.17	>100
C8	0.61 ± 0.05	2.53 ± 0.22	C18	0.27 ± 0.02	1.97 ± 0.17
C9	0.86 ± 0.13	3.01 ± 0.28	C19	0.54 ± 0.04	2.16 ± 0.19
C10	3.88 ± 0.34	6.05 ± 0.56	C20	83.6 ± 7.85	>100
C0A	0.11 ± 0.01	0.75 ± 0.06	C0B	0.14 ± 0.01	1.57 ± 0.11
C0A (lit)	0.11 ± 0.02	0.58 ± 0.07	C0B (lit)	0.15 ± 0.01	1.75 ± 0.12
Erlotinib	0.06 ± 0.01	8.14 ± 0.78	Vemurafenib	0.03 ± 0.004	0.21 ± 0.02

compounds were docked into the active site of the receptor B-Raf. According to previous researches, two crystal structures of B-Raf (PDB Code: 3PSD.pdb²⁹ and 2FB8.pdb¹⁹) were chosen. The receptor and ligands were prepared and the site sphere was chosen due to the ligand binding location. The same as previous study,²³ the results of models using 3PSD and 2FB8 were almost the same due to the generation of random conformations and the similarity of the active sites. The CDocker Interaction Energy (interaction energy between the ligand and the receptor) agreed with the B-Raf inhibitory trend for all the synthesized compounds. Both 2D and 3D maps of the most potent compound **C6** with 3PSD were depicted in Figure 3 with 2D maps of three comparisons **C7**, **C16** and **C15**.

The binding pattern of **C6** and **C7** was similar to previous researches with the typical π - π interaction between ring A/C and PHE583. Compound **C6** formed this π - π interaction between ring A and PHE583 (distance: 6.41 Å) while the stretched ring B possessed interactions with more residues, improving the binding situation. Compound **C7** formed this π - π interaction between ring C and PHE583 (distance: 4.47 Å) with π - π interaction between ring C and TRP531 (distance: 5.29 Å) and π -cation interaction between ring B and LYS483 (distance: 5.68 Å). Thus, **C7** was the nearest one

to the previous best compounds while **C6** broke the limit by stretching the backbone. Actually, **C16** was also this pattern because PHE583 was between its ring A and ring C. Although the interaction was not so strong to form π - π interaction, a hydrogen bonding interaction (O...H-N: 2.15 Å, 164.566°) between dioxin moiety and ASN580 remedied this weakness. **C15** belonged to a totally different pattern for PHE583 escaped from the plane of ring A and ring C. The nice bioactivity might, instead, rely on π -cation interaction between ring B and LYS483 (distance: 5.19 Å) and hydrogen bonding interaction (O...H-N: 2.30 Å, 126.234°) between dioxin moiety and ASN580.

According to receptor surface model shown in Figure 4, the molecules were well embedded in the active pocket including VAL471, PHE583, ALA481, THR529, LEU514 and ASN581. The stretching and distortion on ring B of **C6** resulted in a deeper occupation into the active pocket.

2.4. 3D QSAR model

Since the challenging design affected the backbone, a new 3D QSAR model was built. With the same method as our previous researches,³⁰ Create 3D QSAR protocol of Discovery Studio 3.5

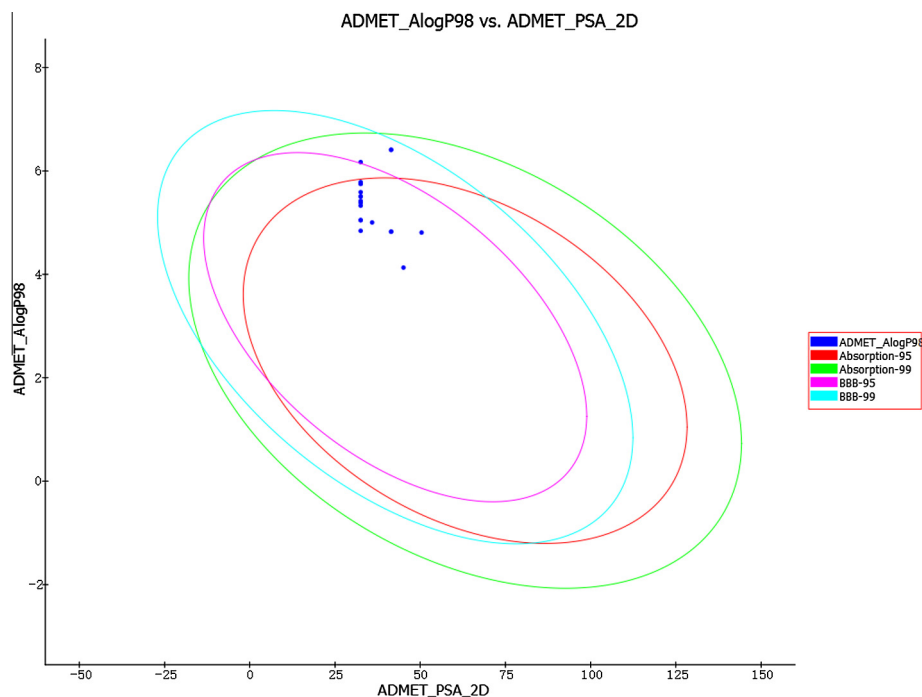


Figure 1. ADMET properties predicted for the twenty compounds **C1–C20**. Compounds located inside the innermost oval are better for this parameter. The three compounds outside the innermost oval were **C6**, **C15** and **C18**.

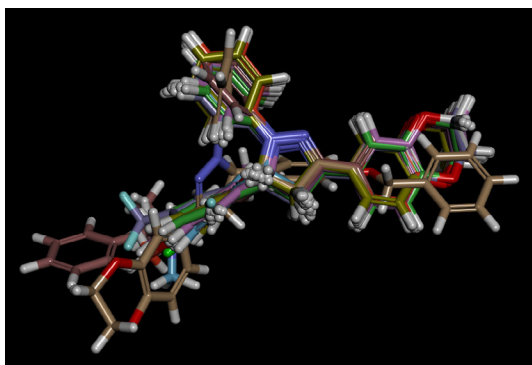


Figure 2. Molecular overlap of compounds **C1–C20**. **C15** has a reversed conformation.

was utilized to perform the 3D QSAR of all twenty compounds based on the definite IC_{50} values. By convention, the values were changed into pIC_{50} scale ($-\log IC_{50}$). Diverse Molecules method in Discovery Studio 3.5 was utilized to choose training set and test set. The alignment conformation of each molecule with lowest energy in the docked results of CDocker protocol was aligned by the substructure **C1**. The maps of 3D QSAR model were shown in Figure 5.

The 3D QSAR model was acceptable with the correlation coefficient r^2 between observed activity of testing set and training set found to be 0.884. Molecules aligned with the *iso*-surfaces of the model coefficients on electrostatic potential grids (Fig. 5-left) and Van der Waals grids (Fig. 5-right) were listed. Electrostatic map indicated regions where electron-withdrawing (red) or electron-donating (blue) groups would increase activity while steric map indicated areas where steric bulk would increase (green) or decrease (yellow) activity. According to the maps, ring A containing dioxin had reached a relatively ideal situation while ring C would still have large potential to be modified. A promising orientation was making ring C slightly larger with electron-donating substitutes. As for ring B, *meta*-position requested a larger electron-withdrawing group while *para*-position asked for a group with appropriate size and slighter electronic influence. However, after skipping out the residues around ring B, the outer space could bear further modifications.

3. Conclusions

To sum up, a series of compounds (**C1–C20**) 3-(2,3-dihydrobenzo[*b*][1,4]dioxin-6-yl)-5-aryl-1-phenyl-4,5-dihydro-1*H*-pyrazoles have been synthesized. Their B-Raf inhibitory and anti-proliferation activities were evaluated. Compound **C6** displayed the most potent biological activity against B-Raf^{V600E} and

Table 2
Selectivity (against B-Raf^{WT}, C-Raf, EGFR and MCF-7 cell line) and cytotoxicity (against NIH3T3 cell line) of representative compounds (**C6**, **C16**, **C15**, **C7**, **C5** and **C18**)

Compounds	IC_{50} (μ M) B-Raf ^{WT}	IC_{50} (μ M) C-Raf	IC_{50} (μ M) EGFR	GI_{50} (μ M) MCF-7	GI_{50} (μ M) NIH3T3
C6	1.06 ± 0.09	6.80 ± 0.55	7.92 ± 0.65	14.8 ± 1.20	221.5 ± 3.35
C16	0.87 ± 0.06	5.48 ± 0.51	>300	12.1 ± 0.95	256.4 ± 3.52
C15	2.51 ± 0.23	5.17 ± 0.45	9.04 ± 0.87	23.6 ± 2.21	228.5 ± 2.95
C7	1.83 ± 0.15	14.6 ± 1.35	81.2 ± 7.35	55.9 ± 5.15	172.4 ± 2.03
C5	2.62 ± 0.22	22.8 ± 2.10	>300	>100	284.7 ± 3.16
C18	3.37 ± 0.32	8.35 ± 0.81	192 ± 15.4	38.3 ± 3.51	156.3 ± 2.07

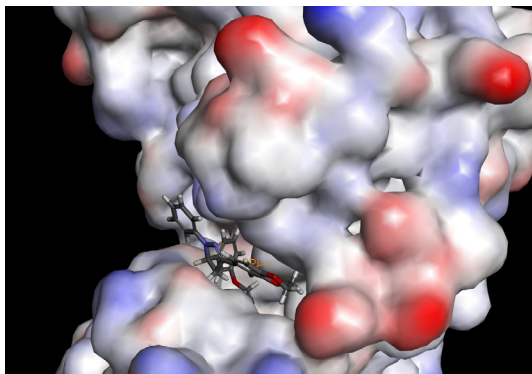


Figure 4. The receptor surface model with C6 in 3PSD.

NMR spectra were reported based on an external hexafluorobenzene reference. NMR data were resolved with MestreNova software. Mass spectra were obtained from an Agilent 6540 UHD Accurate Mass Q-TOF LC/MS.

4.1.2. Compounds

4.1.2.1. General method of synthesis of (*E*)-chalcones (B). To 1-(2,3-dihydrobenzo[*b*][1,4]dioxin-6-yl)ethan-1-one (A) (1 mmol) alcohol solution (5 mL) was added substituted benzaldehyde (1 mmol). After dissolution, 50% NaOH (0.5 mL) was added. After confirming the completion of the reaction by thin layer chromatography, the sediment was filtered, washed with ethanol and dried to obtain chalcone (B).

4.1.2.2. General method of synthesis of 3-(2,3-dihydrobenzo[*b*][1,4]dioxin-6-yl)-5-aryl-1-phenyl-4,5-dihydro-1*H*-pyrazole (C1–C20). Chalcone B (0.5 mmol) and phenylhydrazine (0.5 mmol) in ethanol (5 mL) were refluxed overnight. After the reaction completed, the resultant solid was filtered, washed with ethanol and dried to obtain the corresponding target compound C. In some cases, ultrasonic vibration can contribute to precipitation.

4.1.2.3. 3-(2,3-Dihydrobenzo[*b*][1,4]dioxin-6-yl)-1,5-diphenyl-4,5-dihydro-1*H*-pyrazole (C1). Yellow solid; mp 135–137 °C; yield: 87%; ¹H NMR (400 MHz, CDCl₃) δ 3.08 (dd, 1H, *J* = 16.8, 7.2 Hz), 3.78 (dd, 1H, *J* = 16.8, 12.4 Hz), 4.29 (s, 4H), 5.22 (dd, 1H, *J* = 12.4, 7.2 Hz), 6.76 (t, 1H, *J* = 7.2 Hz), 6.87 (d, 1H, *J* = 8.4 Hz), 7.04 (d, 2H, *J* = 8.0 Hz), 7.14–7.18 (m, 2H), 7.22–7.27 (m, 3H), 7.30–7.35 (m, 4H); ¹³C NMR (100 MHz, CDCl₃) δ 43.9, 64.5, 64.7 (d, *J* = 2.0 Hz), 113.4, 114.9, 117.5, 119.0, 119.5, 126.0,

126.6, 127.6, 129.0, 129.2, 142.9, 143.7, 144.4, 145.2, 146.6; HRMS (ESI-TOF) *m/z*: [M+H]⁺ Calcd for C₂₃H₂₁N₂O₂ 357.1598, Found 357.1594.

4.1.2.4. 3-(2,3-Dihydrobenzo[*b*][1,4]dioxin-6-yl)-5-(naphthalen-1-yl)-1-phenyl-4,5-dihydro-1*H*-pyrazole (C2). Yellow solid; mp 112–114 °C; yield: 81%; ¹H NMR (400 MHz, CDCl₃) δ 3.10 (dd, 1H, *J* = 16.4, 7.6 Hz), 4.01 (dd, 1H, *J* = 16.8, 12.8 Hz), 4.27 (s, 4H), 5.89–5.93 (m, 1H), 6.76 (t, 1H, *J* = 7.2 Hz), 6.85 (d, 1H, *J* = 8.4 Hz), 7.03 (d, 2H, *J* = 8.0 Hz), 7.15 (t, 2H, *J* = 7.6 Hz), 7.22–7.26 (m, 2H), 7.35–7.44 (m, 2H), 7.54–7.64 (m, 2H), 7.78 (d, 1H, *J* = 8.0 Hz), 7.94 (d, 1H, *J* = 8.0 Hz), 8.10 (d, 1H, *J* = 8.4 Hz); ¹³C NMR (100 MHz, CDCl₃) δ 43.0, 64.5, 64.7, 113.4, 114.9, 117.5, 119.0, 119.5, 123.1, 125.9, 126.1, 126.5, 126.6, 128.1, 129.1, 129.4, 130.1, 134.5, 136.9, 143.7, 144.5, 145.3, 147.1; HRMS (ESI-TOF) *m/z*: [M+H]⁺ Calcd for C₂₇H₂₃N₂O₂ 407.1754, Found 407.1751.

4.1.2.5. 3-(2,3-Dihydrobenzo[*b*][1,4]dioxin-6-yl)-5-(naphthalen-2-yl)-1-phenyl-4,5-dihydro-1*H*-pyrazole (C3). Yellow solid; mp 171–172 °C; yield: 88%; ¹H NMR (400 MHz, CDCl₃) δ 3.15 (dd, 1H, *J* = 17.2, 7.6 Hz), 3.85 (dd, 1H, *J* = 17.2, 12.4 Hz), 4.28 (s, 4H), 5.38 (dd, 1H, *J* = 17.2, 12.4 Hz), 6.75 (t, 1H, *J* = 7.2 Hz), 6.88 (d, 1H, *J* = 8.0 Hz), 7.08–7.17 (m, 4H), 7.24–7.26 (m, 2H), 7.43–7.49 (m, 3H), 7.79–7.84 (m, 4H); ¹³C NMR (100 MHz, CDCl₃) δ 43.9, 64.5, 64.7, 65.0, 113.5, 114.9, 117.6, 119.1, 119.5, 124.0, 124.8, 126.1, 126.5, 126.6, 127.9, 128.0, 129.0, 129.4, 133.1, 133.7, 140.3, 143.7, 144.5, 145.4, 146.7; HRMS (ESI-TOF) *m/z*: [M+H]⁺ Calcd for C₂₇H₂₃N₂O₂ 407.1754, Found 407.1753.

4.1.2.6. 3-(2,3-Dihydrobenzo[*b*][1,4]dioxin-6-yl)-5-(2-fluorophenyl)-1-phenyl-4,5-dihydro-1*H*-pyrazole (C4). Yellow solid; mp 139–141 °C; yield: 82%; ¹H NMR (400 MHz, CDCl₃) δ 3.06 (dd, 1H, *J* = 16.8, 6.4 Hz), 3.84 (dd, 1H, *J* = 17.2, 12.4 Hz), 4.28 (s, 4H), 5.54 (dd, 1H, *J* = 12.4, 6.8 Hz), 6.77–6.80 (m, 1H), 6.87 (d, 1H, *J* = 8.4 Hz), 7.01–7.04 (m, 3H), 7.09–7.13 (m, 1H), 7.17–7.26 (m, 5H); ¹³C NMR (100 MHz, CDCl₃) δ 42.5, 58.7 (d, *J* = 3.0 Hz), 64.5, 64.7, 113.2, 114.9, 115.6, 115.8, 117.5, 119.1, 119.5, 124.9 (d, *J* = 4.0 Hz), 126.4, 127.7 (d, *J* = 4.0 Hz), 129.1 (d, *J* = 4.0 Hz), 129.3 (d, *J* = 6.0 Hz), 143.7, 144.5, 144.9, 147.1, 158.7, 161.1; ¹⁹F NMR (376.38 MHz, CDCl₃) δ –118.90; HRMS (ESI-TOF) *m/z*: [M+H]⁺ Calcd for C₂₃H₂₀FN₂O₂ 375.1503, Found 375.1502.

4.1.2.7. 3-(2,3-Dihydrobenzo[*b*][1,4]dioxin-6-yl)-5-(3-methoxyphenyl)-1-phenyl-4,5-dihydro-1*H*-pyrazole (C5). Yellow solid; mp 125–127 °C; yield: 85%; ¹H NMR (400 MHz, CDCl₃) δ 3.08 (dd, 1H, *J* = 16.8, 7.2 Hz), 3.73–3.80 (m, 4H), 4.28 (s, 4H), 5.17 (dd, 1H, *J* = 12.0, 7.2 Hz), 6.75–6.81 (m, 2H), 6.86–6.92 (m,

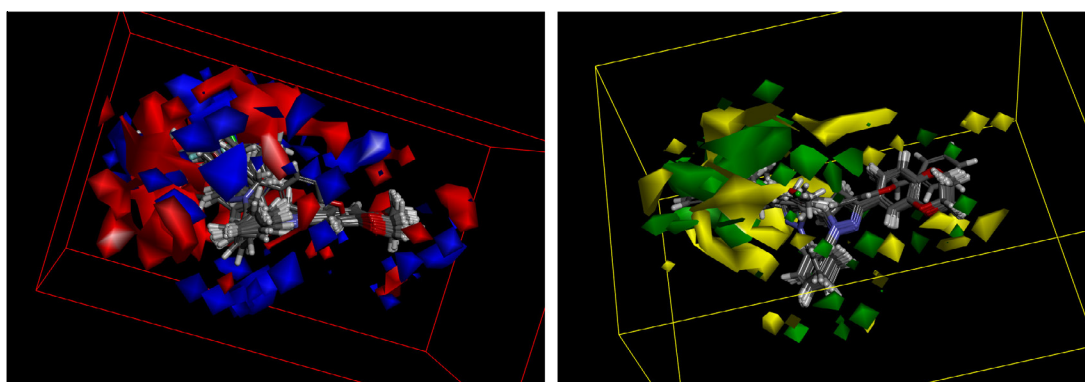


Figure 5. 3D-QSAR of compounds C1–C20. In the maps red contours mean electron-withdrawing group is expected to increase activity while blue contours mean electron-donating group is better. Green areas mean steric bulk is better while yellow areas mean small groups are helpful.

3H), 7.05 (d, 2H, $J = 8.4$ Hz), 7.17 (t, 2H, $J = 8.0$ Hz), 7.22–7.26 (m, 3H); ^{13}C NMR (100 MHz, CDCl_3) δ 43.9, 55.4, 64.5, 64.7, 64.8, 111.5, 113.1, 113.5, 114.9, 117.5, 118.3, 119.1, 119.5, 126.6, 129.0, 130.3, 143.7, 144.4, 144.6, 145.4, 146.7, 160.4; HRMS (ESI-TOF) m/z : $[\text{M}+\text{H}]^+$ Calcd for $\text{C}_{24}\text{H}_{23}\text{N}_2\text{O}_3$ 387.1703, Found 387.1707.

4.1.2.8. 5-(3-(Benzyloxy)phenyl)-3-(2,3-dihydrobenzo[*b*][1,4]-dioxin-6-yl)-1-phenyl-4,5-dihydro-1H-pyrazole (C6).

Brown solid; mp 63–65 °C; yield: 79%; ^1H NMR (400 MHz, CDCl_3) δ 3.07 (dd, 1H, $J = 17.2$, 7.6 Hz), 3.76 (dd, 1H, $J = 17.2$, 12.4 Hz), 4.28 (s, 4H), 5.00 (s, 2H), 5.17 (dd, 1H, $J = 12.0$, 7.2 Hz), 6.77 (t, 1H, $J = 7.2$ Hz), 6.87 (d, 2H, $J = 8.0$ Hz), 6.93 (d, 2H, $J = 8.4$ Hz), 7.05 (d, 2H, $J = 8.0$ Hz), 7.15–7.40 (m, 11H); ^{13}C NMR (100 MHz, CDCl_3) δ 43.9, 64.5, 64.7 (d, $J = 2.0$ Hz), 70.1, 112.4, 113.4, 114.0, 114.9, 117.5, 118.6, 119.0, 119.5, 126.6, 127.8, 128.1, 128.7, 129.0, 130.4, 136.9, 143.6, 144.4, 144.7, 145.3, 146.7, 159.6; HRMS (ESI-TOF) m/z : $[\text{M}+\text{H}]^+$ Calcd for $\text{C}_{30}\text{H}_{27}\text{N}_2\text{O}_3$ 463.2016, Found 463.2010.

4.1.2.9. 5-(3-Chlorophenyl)-3-(2,3-dihydrobenzo[*b*][1,4]dioxin-6-yl)-1-phenyl-4,5-dihydro-1H-pyrazole (C7).

Brown solid; mp 66–68 °C; yield: 72%; ^1H NMR (400 MHz, CDCl_3) δ 3.06 (dd, 1H, $J = 16.8$, 7.2 Hz), 3.79 (dd, 1H, $J = 17.2$, 12.4 Hz), 4.28 (s, 4H), 5.18 (dd, 1H, $J = 12.4$, 7.2 Hz), 6.79 (t, 1H, $J = 7.2$ Hz), 6.87 (d, 1H, $J = 8.0$ Hz), 7.02 (d, 2H, $J = 8.4$ Hz), 7.16–7.26 (m, 7H), 7.33 (s, 1H); ^{13}C NMR (100 MHz, CDCl_3) δ 43.8, 64.2, 64.5, 64.7, 113.4, 114.9, 117.6, 119.3, 119.5, 124.2, 126.2, 126.4, 128.0, 129.1, 130.6, 135.1, 143.7, 144.6, 145.1 (t, $J = 4.0$ Hz), 146.6; HRMS (ESI-TOF) m/z : $[\text{M}+\text{H}]^+$ Calcd for $\text{C}_{23}\text{H}_{20}\text{ClN}_2\text{O}_2$ 391.1208, Found 391.1197.

4.1.2.10. 3-(2,3-Dihydrobenzo[*b*][1,4]dioxin-6-yl)-1-phenyl-5-(*p*-tolyl)-4,5-dihydro-1H-pyrazole (C8).

Yellow solid; mp 133–135 °C; yield: 83%; ^1H NMR (400 MHz, CDCl_3) δ 2.32 (s, 3H), 3.06 (dd, 1H, $J = 17.2$, 7.6 Hz), 3.76 (dd, 1H, $J = 16.8$, 12.0 Hz), 4.28 (s, 4H), 5.19 (dd, 1H, $J = 12.0$, 7.2 Hz), 6.75 (t, 1H, $J = 7.2$ Hz), 6.87 (t, 1H, $J = 8.4$ Hz), 7.05 (d, 2H, $J = 8.4$ Hz), 7.12–7.26 (m, 8H); ^{13}C NMR (100 MHz, CDCl_3) δ 21.2, 44.0, 64.5, 64.7, 113.4, 114.8, 117.5, 118.9, 119.5, 126.0, 126.7, 129.0, 129.9, 137.3, 139.9, 143.7, 144.4, 146.3, 146.6; HRMS (ESI-TOF) m/z : $[\text{M}+\text{H}]^+$ Calcd for $\text{C}_{24}\text{H}_{23}\text{N}_2\text{O}_2$ 358.1676, Found 358.1681.

4.1.2.11. 5-(4-Bromophenyl)-3-(2,3-dihydrobenzo[*b*][1,4]-dioxin-6-yl)-1-phenyl-4,5-dihydro-1H-pyrazole (C9).

Yellow solid; mp 126–128 °C; yield: 87%; ^1H NMR (400 MHz, CDCl_3) δ 3.03 (dd, 1H, $J = 16.8$, 7.2 Hz), 3.78 (dd, 1H, $J = 16.8$, 12.4 Hz), 4.28 (s, 4H), 5.19 (dd, 1H, $J = 12.4$, 7.2 Hz), 6.78 (t, 1H, $J = 7.2$ Hz), 6.87 (d, 1H, $J = 8.0$ Hz), 7.01 (d, 2H, $J = 8.0$ Hz), 7.15–7.26 (m, 6H), 7.45 (d, 2H, $J = 8.0$ Hz); ^{13}C NMR (100 MHz, CDCl_3) δ 64.5, 64.7, 105.2, 114.9, 117.6, 119.3, 122.7, 125.4, 126.7, 127.7, 129.2, 129.7, 130.4, 131.8, 140.0, 143.2, 143.8 (d, $J = 3.0$ Hz), 151.9; HRMS (ESI-TOF) m/z : $[\text{M}+\text{H}]^+$ Calcd for $\text{C}_{23}\text{H}_{20}\text{BrN}_2\text{O}_2$ 435.0703, Found 435.0702.

4.1.2.12. 3-(2,3-Dihydrobenzo[*b*][1,4]dioxin-6-yl)-5-(4-fluorophenyl)-1-phenyl-4,5-dihydro-1H-pyrazole (C10).

Brown solid; mp 75–77 °C; yield: 86%; ^1H NMR (400 MHz, CDCl_3) δ 3.04 (dd, 1H, $J = 16.8$, 6.8 Hz), 3.77 (dd, 1H, $J = 16.8$, 12.4 Hz), 4.28 (s, 4H), 5.21 (dd, 1H, $J = 12.0$, 6.8 Hz), 6.78 (t, 1H, $J = 7.2$ Hz), 6.87 (d, 1H, $J = 8.8$ Hz), 6.99–7.03 (m, 4H), 7.15–7.30 (m, 6H); ^{13}C NMR (100 MHz, CDCl_3) δ 43.8, 64.0, 64.5, 64.7, 113.4, 114.9, 116.0, 116.2, 117.6, 119.2, 119.5, 126.4, 127.7 (d, $J = 8.0$ Hz), 129.0, 138.5 (d, $J = 3.0$ Hz), 143.7, 144.5, 145.0, 146.6, 161.0, 163.4; ^{19}F NMR (376.38 MHz, CDCl_3) δ –114.93; HRMS (ESI-TOF) m/z : $[\text{M}+\text{H}]^+$ Calcd for $\text{C}_{23}\text{H}_{20}\text{FN}_2\text{O}_2$ 375.1503, Found 375.1501.

4.1.2.13. 5-(4-Chlorophenyl)-3-(2,3-dihydrobenzo[*b*][1,4]-dioxin-6-yl)-1-phenyl-4,5-dihydro-1H-pyrazole (C11).

White solid; mp 116–118 °C; yield: 85%; ^1H NMR (400 MHz, CDCl_3) δ 3.03 (dd, 1H, $J = 16.8$, 7.2 Hz), 3.81 (dd, 1H, $J = 17.2$, 12.4 Hz), 4.28 (s, 4H), 5.20 (dd, 1H, $J = 12.0$, 7.2 Hz), 6.78 (t, 1H, $J = 7.2$ Hz), 6.87 (d, 1H, $J = 8.0$ Hz), 7.01 (d, 2H, $J = 8.0$ Hz), 7.15–7.31 (m, 8H); ^{13}C NMR (100 MHz, CDCl_3) δ 43.8, 64.0, 64.5, 64.7, 113.4, 114.9, 117.6, 119.3, 119.5, 126.4, 127.5, 129.1, 129.4, 133.4, 141.3, 143.7, 144.5, 145.0, 146.6; HRMS (ESI-TOF) m/z : $[\text{M}+\text{H}]^+$ Calcd for $\text{C}_{23}\text{H}_{20}\text{ClN}_2\text{O}_2$ 391.1208, Found 391.1211.

4.1.2.14. 3-(2,3-Dihydrobenzo[*b*][1,4]dioxin-6-yl)-5-(4-methoxyphenyl)-1-phenyl-4,5-dihydro-1H-pyrazole (C12).

Yellow solid; mp 113–115 °C; yield: 80%; ^1H NMR (400 MHz, CDCl_3) δ 3.05 (dd, 1H, $J = 17.2$, 7.2 Hz), 3.71–3.78 (m, 4H), 4.28 (s, 4H), 5.18 (dd, 1H, $J = 12.0$, 7.2 Hz), 6.75 (t, 1H, $J = 7.2$ Hz), 6.84–6.88 (m, 3H), 7.05 (d, 2H, $J = 8.0$ Hz), 7.14–7.26 (m, 6H); ^{13}C NMR (100 MHz, CDCl_3) δ 44.0, 55.4, 64.2, 64.5, 64.7, 113.5, 114.6, 114.8, 117.5, 119.0, 119.5, 127.2, 129.0, 134.9, 143.7, 144.4, 145.3, 146.4, 159.1; HRMS (ESI-TOF) m/z : $[\text{M}+\text{H}]^+$ Calcd for $\text{C}_{24}\text{H}_{23}\text{N}_2\text{O}_3$ 387.1703, Found 387.1699.

4.1.2.15. 3-(2,3-Dihydrobenzo[*b*][1,4]dioxin-6-yl)-5-(4-iodophenyl)-1-phenyl-4,5-dihydro-1H-pyrazole (C13).

Yellow solid; mp 150–152 °C; yield: 80%; ^1H NMR (400 MHz, $\text{DMSO}-d_6$) δ 3.03 (dd, 1H, $J = 17.2$, 7.2 Hz), 3.77 (dd, 1H, $J = 17.2$, 12.4 Hz), 4.28 (s, 4H), 5.17 (dd, 1H, $J = 12.4$, 7.2 Hz), 6.78 (t, 1H, $J = 7.2$ Hz), 6.87 (d, 1H, $J = 8.0$ Hz), 7.01 (d, 2H, $J = 8.4$ Hz), 7.07 (d, 2H, $J = 7.6$ Hz), 7.15–7.26 (m, 4H), 7.65 (d, 2H, $J = 8.0$ Hz); ^{13}C NMR (100 MHz, $\text{DMSO}-d_6$) δ 43.7, 64.1, 64.5, 64.7, 93.0, 113.4, 114.9, 117.6, 119.3, 119.5, 125.4, 126.3, 128.1, 129.1, 130.5, 137.8, 138.3, 142.6, 143.7, 144.5, 145.0, 146.6; HRMS (ESI-TOF) m/z : $[\text{M}+\text{H}]^+$ Calcd for $\text{C}_{23}\text{H}_{20}\text{IN}_2\text{O}_2$ 483.0564, Found 483.0558.

4.1.2.16. 3-(2,3-Dihydrobenzo[*b*][1,4]dioxin-6-yl)-5-(4-(methylthio)phenyl)-1-phenyl-4,5-dihydro-1H-pyrazole (C14).

Yellow solid; mp 182–184 °C; yield: 92%; ^1H NMR (400 MHz, $\text{DMSO}-d_6$) δ 2.46 (s, 3H), 3.05 (dd, 1H, $J = 16.8$, 7.2 Hz), 3.76 (dd, 1H, $J = 16.8$, 12.4 Hz), 4.28 (s, 4H), 5.19 (dd, 1H, $J = 12.4$, 7.2 Hz), 6.76 (t, 1H, $J = 7.2$ Hz), 6.87 (d, 1H, $J = 8.4$ Hz), 7.03 (d, 2H, $J = 8.0$ Hz), 7.15–7.26 (m, 8H); ^{13}C NMR (100 MHz, $\text{DMSO}-d_6$) δ 16.0, 43.8, 64.3, 64.5, 64.7, 113.5, 114.9, 117.6, 119.1, 119.5, 126.6, 127.4, 129.0, 137.8, 139.8, 143.7, 144.5, 145.2, 146.6; HRMS (ESI-TOF) m/z : $[\text{M}+\text{H}]^+$ Calcd for $\text{C}_{24}\text{H}_{23}\text{N}_2\text{O}_2\text{S}$ 403.1475, Found 403.1480.

4.1.2.17. 5-(4-(Benzyloxy)phenyl)-3-(2,3-dihydrobenzo[*b*][1,4]-dioxin-6-yl)-1-phenyl-4,5-dihydro-1H-pyrazole (C15).

Yellow solid; mp 136–138 °C; yield: 90%; ^1H NMR (400 MHz, CDCl_3) δ 3.05 (dd, 1H, $J = 16.8$, 7.2 Hz), 3.75 (dd, 1H, $J = 16.8$, 12.0 Hz), 4.28 (s, 4H), 5.02 (s, 2H), 5.18 (dd, 1H, $J = 12.0$, 7.2 Hz), 6.76 (t, 1H, $J = 7.2$ Hz), 6.87 (d, 1H, $J = 8.8$ Hz), 6.93 (d, 2H, $J = 8.4$ Hz), 7.05 (d, 2H, $J = 7.6$ Hz), 7.16 (t, 2H, $J = 8.4$ Hz), 7.22–7.26 (m, 3H), 7.30–7.43 (m, 6H); ^{13}C NMR (100 MHz, CDCl_3) δ 43.9, 64.2, 64.5 (d, $J = 5.0$ Hz), 64.6 (d, $J = 3.0$ Hz), 70.2, 104.6, 113.4, 114.8, 115.0 (d, $J = 3.0$ Hz), 115.5, 117.5 (d, $J = 5.0$ Hz), 119.0, 119.4 (d, $J = 8.0$ Hz), 125.5, 126.7, 127.7 (d, $J = 2.0$ Hz), 128.1, 128.3, 128.7 (d, $J = 2.0$ Hz), 129.0 (d, $J = 5.0$ Hz), 130.2, 135.2, 137.1, 143.6, 143.8, 144.4, 145.2, 146.6, 158.3, 159.0; HRMS (ESI-TOF) m/z : $[\text{M}+\text{H}]^+$ Calcd for $\text{C}_{30}\text{H}_{27}\text{N}_2\text{O}_3$ 463.2016, Found 463.2019.

4.1.2.18. 4-(3-(2,3-Dihydrobenzo[*b*][1,4]dioxin-6-yl)-1-phenyl-4,5-dihydro-1H-pyrazol-5-yl)-*N,N*-dimethylaniline (C16).

Yellow solid; mp 168–170 °C; yield: 80%; ^1H NMR (400 MHz, CDCl_3) δ 2.92 (s, 6H), 3.06 (dd, 1H, $J = 16.8$, 7.2 Hz), 3.72 (dd, 1H, $J = 16.8$, 12.0 Hz), 4.28 (s, 4H), 5.14 (dd, 1H, $J = 12.4$,

7.6 Hz), 6.66–6.70 (m, 2H), 6.72–6.76 (m, 1H), 6.85–6.88 (m, 1H), 7.06–7.09 (m, 2H), 7.14–7.26 (m, 6H); ^{13}C NMR (100 MHz, CDCl_3) δ 40.7, 43.9, 64.4, 64.5, 64.7, 113.1, 113.5, 114.8, 117.5, 118.8, 119.4, 126.9, 128.9, 130.5, 143.6, 144.2, 145.4, 146.6, 150.1; HRMS (ESI-TOF) m/z : $[\text{M}+\text{H}]^+$ Calcd for $\text{C}_{25}\text{H}_{26}\text{N}_3\text{O}_2$ 400.2020, Found 400.2015.

4.1.2.19. 3-(2,3-Dihydrobenzo[*b*][1,4]dioxin-6-yl)-1-phenyl-5-(4-(trifluoromethyl)phenyl)-4,5-dihydro-1H-pyrazole (C17).

Yellow solid; mp 111–113 °C; yield: 77%; ^1H NMR (400 MHz, CDCl_3) δ 3.05 (dd, 1H, $J = 16.8, 7.2$ Hz), 3.82 (dd, 1H, $J = 17.2, 12.4$ Hz), 4.28 (s, 4H), 5.29 (dd, 1H, $J = 12.0, 6.8$ Hz), 6.79 (t, 1H, $J = 7.6$ Hz), 6.88 (d, 1H, $J = 8.4$ Hz), 6.99–7.02 (m, 2H), 7.16–7.26 (m, 4H), 7.44 (d, 2H, $J = 8.0$ Hz), 7.59 (d, 2H, $J = 8.4$ Hz); ^{13}C NMR (100 MHz, CDCl_3) δ 43.7, 64.1, 64.5, 64.7, 113.4, 114.9, 117.6, 119.4, 119.5, 126.2, 126.3 (q, $J = 3.0$ Hz), 126.5, 129.2, 143.7, 144.6, 144.9, 146.6, 146.8 (d, $J = 1.0$ Hz); ^{19}F NMR (376.38 MHz, CDCl_3) δ –62.53; HRMS (ESI-TOF) m/z : $[\text{M}+\text{H}]^+$ Calcd for $\text{C}_{24}\text{H}_{20}\text{F}_3\text{N}_2\text{O}_2$ 425.1471, Found 425.1468.

4.1.2.20. 5-(3,4-Dichlorophenyl)-3-(2,3-dihydrobenzo[*b*][1,4]dioxin-6-yl)-1-phenyl-4,5-dihydro-1H-pyrazole (C18).

Brown solid; mp 65–67 °C; yield: 75%; ^1H NMR (400 MHz, CDCl_3) δ 3.03 (dd, 1H, $J = 17.2, 7.2$ Hz), 3.79 (dd, 1H, $J = 17.2, 12.4$ Hz), 4.28 (s, 4H), 5.16 (dd, 1H, $J = 12.4, 7.2$ Hz), 6.80 (t, 1H, $J = 7.2$ Hz), 6.87 (d, 1H, $J = 8.4$ Hz), 7.00 (d, 2H, $J = 8.0$ Hz), 7.14–7.26 (m, 5H), 7.32–7.43 (m, 3H); ^{13}C NMR (100 MHz, CDCl_3) δ 43.7, 63.7, 64.5, 64.7, 113.4, 114.9, 117.6, 119.5, 125.4, 126.1, 128.1, 129.2, 131.3, 131.7, 133.4, 143.2, 143.7, 144.6, 144.9, 146.7; HRMS (ESI-TOF) m/z : $[\text{M}+\text{H}]^+$ Calcd for $\text{C}_{23}\text{H}_{19}\text{Cl}_2\text{N}_2\text{O}_2$ 425.0818, Found 425.0820.

4.1.2.21. 3-(2,3-Dihydrobenzo[*b*][1,4]dioxin-6-yl)-5-(3,4-dimethoxyphenyl)-1-phenyl-4,5-dihydro-1H-pyrazole (C19).

Yellow solid; mp 145–147 °C; yield: 81%; ^1H NMR (400 MHz, CDCl_3) δ 3.07 (dd, 1H, $J = 17.2, 8.0$ Hz), 3.72–3.86 (m, 7H), 4.28 (s, 4H), 5.14 (dd, 1H, $J = 12.0, 7.6$ Hz), 6.76–6.83 (m, 3H), 6.86–6.89 (m, 2H), 7.05–7.07 (m, 2H), 7.15–7.19 (m, 2H), 7.22–7.26 (m, 2H); ^{13}C NMR (100 MHz, CDCl_3) δ 44.0, 56.1 (d, $J = 3.0$ Hz), 64.5, 64.7, 64.8, 108.8, 111.6, 113.6, 114.8, 117.5, 118.2, 119.1, 119.5, 126.6, 129.0, 135.5, 143.6, 144.4, 145.5, 146.8, 148.5, 149.7; HRMS (ESI-TOF) m/z : $[\text{M}+\text{H}]^+$ Calcd for $\text{C}_{25}\text{H}_{25}\text{N}_2\text{O}_4$ 417.1809, Found 417.1802.

4.1.2.22. 3-(2,3-Dihydrobenzo[*b*][1,4]dioxin-6-yl)-5-(furan-2-yl)-1-phenyl-4,5-dihydro-1H-pyrazole (C20).

Brown solid; mp 55–57 °C; yield: 80%; ^1H NMR (400 MHz, CDCl_3) δ 3.26 (dd, 1H, $J = 16.8, 6.8$ Hz), 3.64 (dd, 1H, $J = 16.8, 12.4$ Hz), 4.28 (s, 4H), 5.30 (dd, 1H, $J = 12.0, 6.8$ Hz), 6.21 (d, 1H, $J = 3.2$ Hz), 6.29 (dd, 1H, $J = 3.2, 2.0$ Hz), 6.81 (t, 1H, $J = 7.2$ Hz), 6.87–6.90 (m, 1H), 7.14 (d, 2H, $J = 7.6$ Hz), 7.20–7.26 (m, 4H), 7.35 (d, 1H, $J = 1.2$ Hz); ^{13}C NMR (100 MHz, CDCl_3) δ 40.4, 58.3, 64.5, 64.7, 107.0, 110.6, 113.7, 114.9, 117.5, 119.5 (d, $J = 10.0$ Hz), 126.4, 129.0, 142.3, 143.6, 144.5, 145.4, 147.3, 153.9; HRMS (ESI-TOF) m/z : $[\text{M}+\text{Na}]^+$ Calcd for $\text{C}_{21}\text{H}_{18}\text{N}_2\text{O}_3\text{Na}$ 369.1210, Found 369.1209.

4.2. Biological assay

4.2.1. Anti-proliferation assay

WM266.4 melanoma cells²⁷ were cultured in DMEM/10% fetal bovine serum, in 5% CO_2 water saturated atmosphere at 37 °C. Cell suspensions (10,000/mL) were prepared and 100 μL /well dispensed into 96-well plates (Costar) giving 1000 cells/well. The plates were returned to the incubator for 24 h to allow the cells to reattach. These compounds were initially prepared at 20 mM in DMSO. Aliquots (200 μL) were diluted into 20 mL culture

medium giving 200 μM , and 10 serial dilutions of $3 \times$ prepared. Aliquots (100 μL) of each dilution were added to the wells, giving doses ranging from 100 μM to 0.005 μM . After a further incubated at 37 °C for 24 h in a humidified atmosphere with 5% CO_2 , the cell viability was assessed by the conventional 3-(4,5-dimethylthiazol-2-yl)-2,5-diphenyltetrazolium bromide (MTT) reduction assay and carried out strictly according to the manufacturer instructions (Sigma). The absorbance at 590 nm was recorded using LX300 Epson Diagnostic micro-plate reader. Then GI_{50} was calculated using SPSS 13.0 software.

MCF-7 human breast cancer cells were evaluated by the same method as WM266.4 melanoma cells with the results presented in GI_{50} values.

NIH3T3 mouse fibroblast cells were cultured in a 96-well plate at a density of 5×10^5 cells and different concentrations of compounds were respectively added to each well. The incubation was permitted at 37 °C, 5% CO_2 atmosphere for 24 h before the cytotoxicity assessments. 20 μL MTT reagent (4 mg/mL) was added per well 4 h before the end of the incubation. Four hours later, the plate was centrifuged at 1200 rcf for 5 min and the supernatants were removed, each well was added with 200 μL DMSO. The absorbance was measured at a wavelength of 490 nm (OD 490 nm) on an ELISA microplate reader. Three replicate wells were used for each concentration and each assay was measured three times, after which the average of GI_{50} was calculated.

4.2.2. Kinase inhibitory assay

This V600E mutant B-Raf kinase assay was performed in triplicate for each tested compound in this study. Briefly, 7.5 ng Mouse Full-Length GST-tagged BRAF^{V600E} (Invitrogen, PV3849) was pre-incubated at room temperature for 1 h with 1 μL drug and 4 μL assay dilution buffer. The kinase assay was initiated when 5 μL of a solution containing 200 ng recombinant human full length, N-terminal His-tagged MEK1 (Invitrogen), 200 μM ATP, and 30 mM MgCl_2 in assay dilution buffer was added. The kinase reaction was allowed to continue at room temperature for 25 min and was then quenched with 5 μL $5 \times$ protein denaturing buffer (LDS) solution. Protein was further denatured by heating for 5 min at 70 °C. 10 μL of each reaction was loaded into a 15-well, 4–12% pre-cast NuPage gel (Invitrogen) and run at 200 V, and upon completion, the front, which contained excess hot ATP, was cut from the gel and discarded. The gel was then dried and developed onto a phosphor screen. A reaction that contained no active enzyme was used as a negative control, and a reaction without inhibitor was used as the positive control.

Detection of the effect of compounds on cell based pERK1/2 activity in WM266.4 cells was performed using ELISA kits (Invitrogen) and strictly according to the manufacturer instructions.

The wild type B-Raf kinase and C-Raf kinase were evaluated use the same method as V600E mutant B-Raf kinase.

A 1.6 kb cDNA encoded for the EGFR cytoplasmic domain (EGFR-CD, amino acids 645–1186) was cloned into baculoviral expression vectors pBlueBacHis2B and pFASTBacHTc (Huakang Company China), separately. A sequence that encodes (His)₆ was located at the 5' upstream to the EGFR sequences. Sf-9 cells were infected for 3 days for protein expression. Sf-9 cell pellets were solubilized at 0 °C in a buffer at pH 7.4 containing 50 mM HEPES, 10 mM NaCl, 1% Triton, 10 μM ammonium molybdate, 100 μM sodium vanadate, 10 $\mu\text{g}/\text{mL}$ aprotinin, 10 $\mu\text{g}/\text{mL}$ leupeptin, 10 $\mu\text{g}/\text{mL}$ pepstatin, and 16 $\mu\text{g}/\text{mL}$ benzamidine, HCl for 20 min followed by 20 min centrifugation. Crude extract supernatant was passed through an equilibrated Ni-NTA superflow packed column and washed with 10 mM and then 100 mM imidazole to remove non-specifically bound material. Histidine-tagged proteins were eluted with 250 and 500 mM imidazole and dialyzed against 50 mM NaCl, 20 mM HEPES, 10% glycerol and 1 $\mu\text{g}/\text{mL}$ each of aprotinin,

leupeptin, and pepstatin for 2 h. The entire purification procedure was performed at 4 °C or on ice.

EGFR kinase assays was set up to assess the level of autophosphorylation based on DELFIA/Time-Resolved Fluorometry. Compounds **C1–C20** were dissolved in 100% DMSO and diluted to the appropriate concentrations with 25 mM HEPES at pH 7.4. In each well, 10 μ L of compound was incubated with 10 μ L (5 ng for EGFR) of recombinant enzyme (1:80 dilution in 100 mM HEPES) for 10 min at room temperature. Then, 10 μ L of 5 \times buffer (containing 20 mM HEPES, 2 mM MnCl₂, 100 μ M Na₃VO₄, and 1 mM DTT) and 20 μ L of 0.1 mM ATP–50 mM MgCl₂ was added for 1 h. Positive and negative controls were included in each plate by incubation of enzyme with or without ATP–MgCl₂. At the end of incubation, liquid was aspirated and plates were washed three times with wash buffer. A 75 μ L (400 ng) sample of europium-labeled anti-phosphotyrosine antibody was added to each well for another 1 h of incubation. After washing, enhancement solution was added and the signal was detected by Victor (Wallac Inc.) with excitation at 340 nm and emission at 615 nm. The percentage of autophosphorylation inhibition by the compounds was calculated using the following equation: 100% – [(negative control)/(positive control – negative control)]. The IC₅₀ was obtained from curves of percentage inhibition with eight concentrations of compound. As the contaminants in the enzyme preparation are fairly low, the majority of the signal detected by the anti-phosphotyrosine antibody is from EGFR. The experiment was performed in triplicate.

4.3. Experimental protocol of ADMET study

The three-dimensional structures of the aforementioned compounds were constructed using Chem. 3D ultra 12.0 software [Chemical Structure Drawing Standard; Cambridge Soft corporation, USA (2010)]. Then they were minimized a CHARMM based force field the same as in docking study. The ADMET study was conducted using the Calculate Molecular Properties in Small Molecules module of the Discovery Studio (version 3.5). The ADMET properties map and data were provided by the ADMET Descriptors tool.

4.4. Experimental protocol of docking study

The three-dimensional structures of the aforementioned compounds were constructed using Chem. 3D ultra 12.0 software [Chemical Structure Drawing Standard; Cambridge Soft corporation, USA (2010)]. The crystal structures of B-Raf kinase domain bound to SB-590885 (PDB code: 2FB8) and bound to SM7 (PDB code: 3PSD) complex were retrieved from the RCSB Protein Data Bank (<http://www.rcsb.org/pdb/home/home.do>). All bound waters and ligands were eliminated from the protein and the polar hydrogen was added to the proteins. Molecular docking of all twenty compounds as well as **COA** and **COB** was then carried out using the Discovery Studio (version 3.5) as implemented through the graphical user interface CDOCKER protocol.

CDOCKER is an implementation of a CHARMM based molecular docking tool using a half-flexible receptor,³⁰ including the following steps:

- (1) A series of ligands conformations are generated using high temperature molecular dynamics with different random seeds.
- (2) Random orientations of the conformations are generated by translating the center of the ligand to a specified position within the receptor active site, and making a series of random rotations. A softened energy is calculated and the orientation is kept when it is less than a specified limit. This process repeats until either the desired number of

low-energy orientations is obtained, or the test times of bad orientations reached the maximum number.

- (3) Each orientation is subjected to simulated annealing molecular dynamics. The temperature is heated up to a high temperature then cooled to the target temperature. A final energy minimization of the ligand in the rigid receptor using non-softened potential is performed.
- (4) For each of the final pose, the CHARMM energy (interaction energy plus ligand strain) and the interaction energy alone are figured out. The poses are sorted according to CHARMM energy and the top scoring (most negative, thus favorable to binding) poses are retained. The whole B-Raf kinase domain defined as a receptor and the site sphere was selected based on the original ligand binding location, then the original ligand was removed and the ligands prepared by us were placed during the molecular docking procedure. CHARMM was selected as the force field. The molecular docking was performed with a simulated annealing method. The heating steps were 2000 with 700 of heating target temperature. The cooling steps were 5000 with 300 cooling target temperature. Ten molecular docking poses saved for each ligand were ranked according to their dock score function. The pose with the highest -CDOCKER energy was chosen as the most suitable pose.

4.5. Experimental protocol of QSAR model

Among all the 20 compounds, 80% (that is 16) were utilized as a training set for QSAR modeling. The remaining 20% (that is 4) were chosen as an external test subset for validating the reliability of the QSAR model by the Diverse Molecules protocol in Discovery Studio 3.5. The selected test compounds were: **C5**, **C8**, **C10** and **C15**.

The inhibitory activity of the compounds in literatures [IC₅₀ (mol/L)] was initially changed into the minus logarithmic scale [pIC₅₀ (mol/L)] and then used for subsequent QSAR analysis as the response variable.

In Discovery Studio, the CHARMM force field is applied and the electrostatic potential together with the *Van der Waals* potential are treated as separate terms. As the electrostatic potential probe, A + le point charge is used while distance-dependent dielectric constant is used to mimic the solvent effect. As for the *Van der Waals* potential, a carbon atom with a radius of 1.73 Å is used as a probe.

A Partial Least-Squares (PLS) model is built using energy grids as descriptors. QSAR models were built by using the Create 3D QSAR Model protocol in Discovery Studio 3.5.

Supplementary data

Supplementary data associated with this article can be found, in the online version, at <http://dx.doi.org/10.1016/j.bmc.2016.05.012>.

References and notes

1. El-Azab, A. S.; Al-Omar, M. A.; Abdel-Aziz, A. M.; Abdel-Aziz, N. I.; El-Sayed, A. A., et al. *Eur. J. Med. Chem.* **2010**, *45*, 4188.
2. Wellbrock, C.; Karasarides, M.; Marais, R. *Nat. Rev. Mol. Cell Biol.* **2004**, *5*, 875.
3. Li, N.; Batt, D.; Warmuth, M. *Curr. Opin. Invest. Drugs* **2007**, *8*, 452.
4. Hoshino, R.; Chantani, Y.; Yamori, T.; Tsuruo, T.; Oka, H., et al. *Oncogene* **1999**, *18*, 813.
5. Burotto, M.; Chiou, V. L.; Lee, J. M.; Kohn, E. C. *Cancer* **2014**, *120*, 3446.
6. Maurer, G.; Tarkowski, B.; Baccarini, M. *Oncogene* **2011**, *30*, 3477.
7. Davies, H.; Bignell, G. R.; Cox, C.; Stephens, P.; Edkins, S., et al. *Nature* **2002**, *417*, 949.
8. Cohen, Y.; Xing, M.; Mambo, E.; Guo, Z.; Wu, G., et al. *J. Natl Cancer Inst.* **2003**, *95*, 625.
9. Xu, X.; Quiros, R. M.; Gattuso, P.; Ain, K. B.; Prinz, R. A. *Canc. Res.* **2003**, *63*, 4561.

10. Kalinsky, K.; Haluska, F. G. *Expert Rev. Anticancer Ther.* **2007**, *7*, 715.
11. Dhillon, A. S.; Hagan, S.; Rath, O.; Kolch, W. *Oncogene* **2007**, *26*, 3279.
12. Wan, P. T.; Garnet, M. J.; Roe, S. M.; Lee, S.; Niculescu-Duvaz, D., et al. *Cell* **2004**, *116*, 855.
13. Gray-Schopfer, V. C.; Dias, S. D.; Marais, R. *Cancer Metast. Rev.* **2005**, *24*, 367.
14. Sommers, J. A.; Sharma, S.; Doherty, K. M.; Karmakar, P.; Yang, Q., et al. *Canc. Res.* **2005**, *65*, 1223.
15. Karasarides, M.; Chilocheas, A.; Hayward, R.; Niculescu-Duvaz, D.; Scanlon, I., et al. *Oncogene* **2004**, *23*, 6292.
16. Friday, B. B.; Yu, C. R.; Dy, G. K.; Smith, P. D.; Wang, L., et al. *Cancer Res.* **2008**, *68*, 6145.
17. Cui, Y.; Guadagno, T. M. *Oncogene* **2008**, *27*, 3122.
18. Mathieu, S.; Gradl, S. N.; Ren, L.; Wen, Z.; Aliagas, I., et al. *J. Med. Chem.* **2012**, *55*, 2869.
19. King, A. J.; Patrick, D. R.; Batorsky, R. S.; Ho, M. L.; Do, H. T., et al. *Canc. Res.* **2006**, *66*, 11100.
20. De, D. Y. D.; Krogstad, F. M.; Byers, L. D.; Krogstad, D. J. *J. Med. Chem.* **1998**, *41*, 4918.
21. Blackburn, C.; Duffy, M. O.; Gould, A. E.; Kulkarni, B.; Liu, J. X., et al. *Bioorg. Med. Chem. Lett.* **2010**, *20*, 4795.
22. Li, C. Y.; Li, Q. S.; Yan, L.; Sun, X. G.; Wei, R., et al. *Bioorg. Med. Chem.* **2012**, *20*, 3746.
23. Yang, Y. S.; Li, Q. S.; Sun, S.; Zhang, Y. B.; Wang, X. L., et al. *Bioorg. Med. Chem.* **2012**, *20*, 6048.
24. Yang, Y. S.; Zhang, F.; Tang, D. J.; Yang, Y. H.; Zhu, H. L. *PLoS One* **2014**, *9*, e95702.
25. Jonaitis, H.; Urba, V.; Salna, V. *Liet. Fiz. Rinkiny* **1968**, *7*, 861.
26. Dauksas, V.; Milvydiene, G. *Lietuvos TSR Aukstuju Mokyklu Mokslo Darbai, Chem. Ir. Chem. Technol.* **1965**, *7*, 83.
27. Niculescu-Duvaz, D.; Niculescu-Duvaz, I.; Suijkerbuijk, B.; Ménard, D.; Zambon, A., et al. *Bioorg. Med. Chem.* **2010**, *18*, 6934.
28. Kirkpatrick, P. *Nat. Rev. Drug Discovery* **2004**, *3*, 299.
29. Newhouse, B. J.; Hansen, J. D.; Grina, J.; Welch, M.; Topalov, G., et al. *Bioorg. Med. Chem. Lett.* **2011**, *21*, 3488.
30. Wu, G. S.; Robertson, D. H.; Brooks, C. L.; Vieth, M. J. *Comput. Chem.* **2003**, *24*, 1549.